communications biology

A Nature Portfolio journal

Article

https://doi.org/10.1038/s42003-025-07737-1

A nuclear tRNA-derived fragment triggers immunity in Arabidopsis

Sung-Il Kim[1,7], Haomin Lyu[2,8,13], Dinesh S. Pujara[1,9,13], Yogendra Bordiya[1,10,13], Padam S. Bhatt[1], José Mayorga[1], Prince K. Zogli[3,11], Pritha Kundu[3], Haewon Chung[4,12], Xingxing Yan[5], Xiuren Zhang[5], Jonghwan Kim[4], Joe Louis[3], Qingyi Yu[6] & Hong-Gu Kang[1]

In Arabidopsis, effector-triggered immunity (ETI) against avirulent *Pseudomonas syringae* pv. *tomato* (*Pst*) correlates with the rapid, Dicer-Like 1 (DCL1)-dependent nuclear accumulation of a 31-nt 5'-tRNA fragment derived from Asp-tRNA (tRF^{31Asp2}). Several tRFs, including tRF^{31Asp2}, are induced at early stages of infection and associate with AGO2 in the nucleus. Infiltrating Arabidopsis leaves with synthetic tRF^{31Asp2} induces over 500 defense-associated genes, conferring immunity against virulent and avirulent *Pst* as well as aphids, while tRF^{31Asp2} depletion compromises resistance to avirulent *Pst*. The biological activity of tRF^{31Asp2} requires its 5' sequence and predicted stem-loop structure, and its loading into AGO2 or related clade members may contribute to activating defense responses. Chromatin affinity precipitation-sequencing revealed that tRF^{31Asp2} binds specific sequences in defense genes and the *Gypsy* superfamily of LTR retrotransposons, particularly at their primer binding sites (PBS). tRF^{31Asp2} binding appears to modulate transcriptional reprogramming, inducing neighboring tRF-responsive defense genes while suppressing active retrotransposons. Since *Gypsy* retrotransposon proliferation is primed by tRNA binding at PBS, tRF^{31Asp2} may exploit a similar mechanism to coordinate defense responses. Together, these findings reveal a role for DCL1 and tRF^{31Asp2} in regulating plant immunity and transcriptional dynamics at defense-associated loci and retrotransposons.

Plants resist pathogens that breach their passive defenses by detecting conserved Pathogen-Associated Molecular Patterns (PAMPs) and activating PAMP-triggered immunity (PTI). Some pathogens have evolved effectors that, following transport into host cells, facilitate evasion/suppression of PTI[1]. The low resistance observed in plants infected with these pathogens is termed basal immunity. In turn, plants have evolved resistance (R) proteins that interact with their cognate pathogen-encoded effector(s) and induce a robust defense response termed effector-triggered immunity (ETI)[2,3]. Interestingly, most transcripts induced during ETI also accumulate during PTI and basal immunity, albeit with weaker or delayed transcriptional dynamics[4,5]. Recent reports also revealed that the two-tiered immune cascades, ETI and PTI, share a significant number of downstream components, leading to mutual reinforcement[6,7].

RNA silencing is a critical mechanism whereby noncoding small RNAs (sRNAs) regulate gene expression at either the post-transcriptional level, by modulating RNA stability/translatability, or at the transcriptional level, via DNA/histone modification or chromatin remodeling[8]. sRNAs are generated mostly by ribonuclease III-like enzymes, termed Dicer-like (DCL) proteins in plants[6]. Following loading onto Argonaute (AGO) proteins to form RNA-induced silencing complexes (RISC), the sRNA guide strand directs the RISC to complementary RNA targets for post-transcriptional or

[1]Department of Biology, Texas State University, San Marcos, USA. [2]Texas A&M AgriLife Research, Texas A&M University System, Dallas, TX, USA. [3]Department of Entomology & Department of Biochemistry, University of Nebraska, Lincoln, NE, USA. [4]Department of Molecular Biosciences, University of Texas, Austin, TX, USA. [5]Department of Biochemistry & Biophysics, Texas A&M University, College Station, TX, USA. [6]Daniel K. Inouye U.S. Pacific Basin Agricultural Research Center, USDA Agricultural Research Service, Hilo, HI, USA. [7]Present address: Department of Molecular Cellular and Developmental Biology, University of Michigan, Ann Arbor, MI, USA. [8]Present address: Huazhi Biotechnology, Changsha, Hunan, China. [9]Present address: School of Integrated Plant Science, Cornell University, Ithaca, NY, USA. [10]Present address: Biosciences Division, Thermo Fisher Scientific, Austin, TX, USA. [11]Present address: GALY.CO, Boston, MA, USA. [12]Present address: Synthetic biology, Asimov, Boston, MA, USA. [13]These authors contributed equally: Haomin Lyu, Dinesh S. Pujara, Yogendra Bordiya.
e-mail: kang@txstate.edu

transcriptional gene silencing[9]. In Arabidopsis (*Arabidopsis thaliana*), infection with avirulent bacterial pathogen *Pseudomonas syringae* pv. *tomato* (*Pst*) carrying the effector *avrRpt2* (*Pst_avrRpt2*) significantly induces *AGO2*, which together with its homologs *AGO3* and *AGO7* is required for full ETI[10].

In addition to their conventional role in the translational machinery, transfer RNAs (tRNA) exhibit various noncanonical functions such as chromatin organization, DNA repair, and immune responses[11,12]. For instance, a 2′-O-Methyltransferase that modifies tRNA anticodon has been found to play a role in Arabidopsis resistance to *Pst*[13]. Interestingly, sRNAs derived from tRNAs (tsRNAs) are also identified as critical regulatory molecules[14] and found in essentially all species ranging from bacteria to humans[15]. Several classes of tsRNAs have been identified. tRNA-halves (~35 nts), generated via cleavage at the anticodon loop by a ribonuclease such as angiogenin, inhibit protein synthesis by targeting translation machinery[16–18]. The remaining classes, collectively termed tRNA-derived fragments (tRFs), include 5′-tRFs, 3′-tRFs, and i-tRFs[19]. tRFs (<~32 nts) are generated by nucleases like Dicer and RNase Z, and associate with AGOs to mediate post-transcriptional gene silencing[14]. Furthermore, tRFs can be categorized based on their cleavage sites. For example, tRF-5a, tRF-5b, and tRF-5c belong to the group of 5′-tRFs, which are produced by cleaving the D-loop, D-stem, and anticodon stem, respectively[12,20].

Short tRFs that resemble microRNAs in size are associated with Argonaute (AGO) proteins, performing functions similar to microRNAs[15,21]. In human HEK293T cells, for example, upregulating 3′-tRFs leads to the widespread repression of target genes[21]. Rhizobial 3′-tRFs use host AGO1 to repress negative symbiotic regulators in the host[22]. tRFs are also shown to be associated with transposons; 3′-tRFs hinder the replication of endogenous retroviruses (ERVs) by targeting its primer-binding site (PBS)[23], while long 5′-tRFs, especially tRF-5c, in mouse sperm and embryonic stem cells (ESCs) suppress MERVL retrotransposons[24]. Given this mounting evidence of tsRNAs' significance in biology, this study presents an unique function of a long 5′-tRF dependent on DCL1 in plant immunity and provides its underlying mechanical mechanism, in which the tRF physically associates target genes to modulate their transcription.

Results

DCL1, a putative positive regulator in defense responses

We previously showed that some Arabidopsis *ago* and *dcl* mutants are compromised for basal resistance to virulent *Pst* and/or ETI to avirulent *Pst_avrRpt2*[25]. Bacterial growth and the expression of the defense gene *Pathogenesis-related 1* (*PR1*) were monitored in both *dcl1-7* and wild-type (WT) plants to confirm the impact of DCL1 loss on ETI with minimally affecting basal resistance. *dcl1-7* supported significantly higher levels of *Pst_avrRpt2* than WT at 3 day-post-inoculation (dpi), whereas growth of *Pst* in these plants was marginally higher (Fig. 1a). *PR1* expression was significantly dampened in *Pst_avrRpt2*-inoculated *dcl1-7* vs WT at 6 h-post-inoculation (hpi); however, it was marginally different at later points, or at

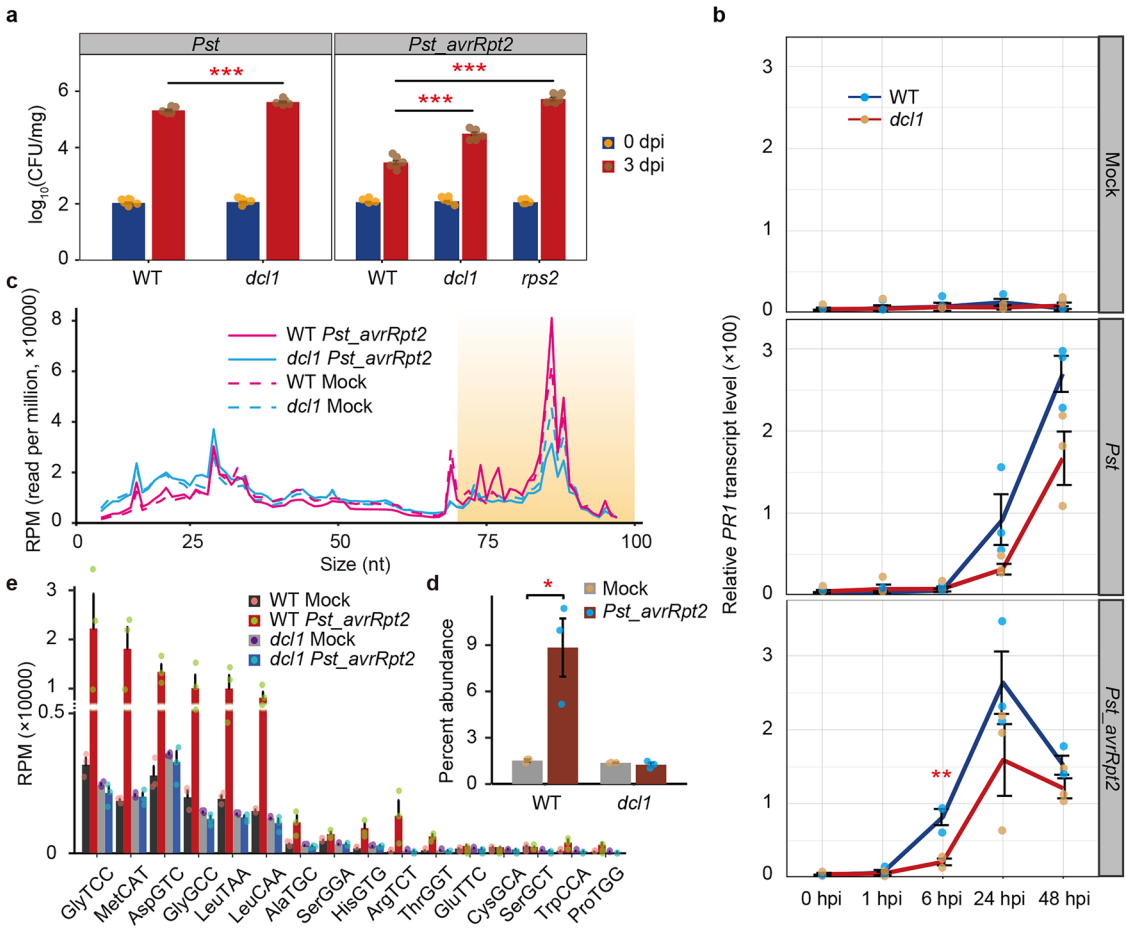

Fig. 1 | Effector-triggered immunity (ETI) to *Pseudomonas syringae* pv. *tomato* (*Pst*) in Arabidopsis is associated with *DCL1* and increased nuclear-localized tRNAs. a Bacterial growth in wild type (WT) and *dcl1-7* at 0 and 3 day-post-infection (dpi) with *Pst* containing or lacking *AvrRpt2* (*Pst_avrRpt2* or *Pst*, respectively); *rps2* is an ETI control. The mean±RSE ($n \geq 9$) from three independent experiments are presented. **b** Relative *PR1* transcription levels measured by qRT-PCR are presented as mean±SD ($n = 3$). **c** Size distribution of nuclear sRNAs (11–100 nts) in WT and *dcl1-7* at 1 h-post-infection (hpi) with *Pst_avrRpt2* or buffer (mock); the y-axis represents a normalized read count in RPM. **d** Percentage of tRNA-aligned reads in 71–100 nts sRNAs. **e** Normalized read counts of tRNA-derived 71–100 nts RNAs as mean±SE ($n = 3$). Significance between indicated pairs is noted; $^{*}P < 0.05$; $^{**}P < 0.01$; $^{***}P < 0.001$ (*t*-test).

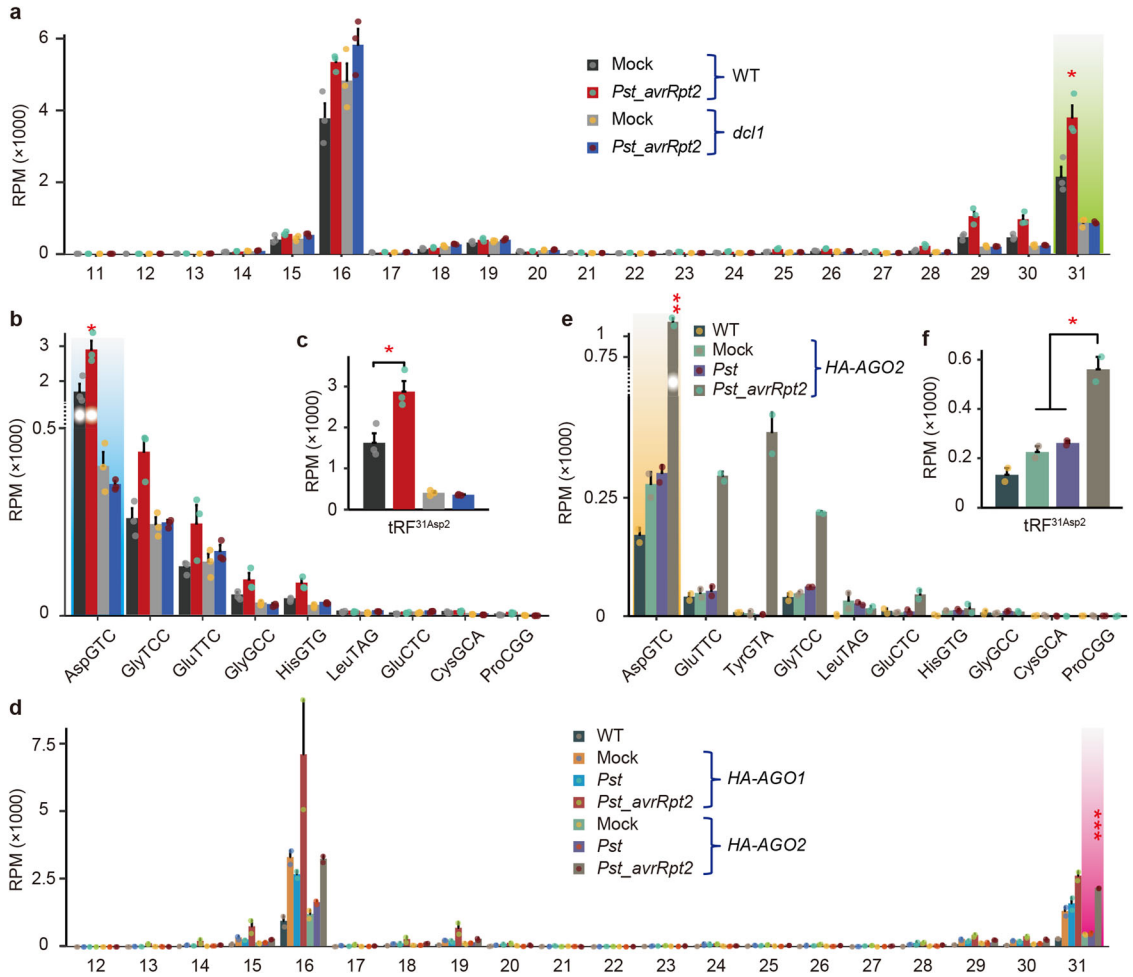

Fig. 2 | AGO2-associated 5′-tRFs display DCL1-dependent induction in Arabidopsis. a–c sRNA-seq analysis of nuclear 5′-tRFs in *Pst_avrRpt2*- or mock-inoculated WT and *dcl1-7* at 1 hpi. **d–f** Nuclear AGO-associated 5′-tRFs in *Pst_avrRpt2*-, *Pst*-, or mock-inoculated *HA-AGO1* and *HA-AGO2* transgenic Arabidopsis at 1 hpi were identified by sRIP-seq via α-HA; WT was the negative control. The y-axis represents a normalized read count in RPM. Size distribution of 5′-tRFs (**a**, **d**). Normalized read counts of 31 nt-long 5′-tRFs originated from each tRNA isodecoder (**b**, **e**) and of a representative *Pst_avrRpt2*-inducible, DCL1-dependent 5′-tRF (tRF^{31Asp2}) (**c**, **f**). The mean ± SE is presented ($n = 3$, **a–c**; $n = 2$, **d–f**). Significance from mock noted for highlighted samples only; $^{*}P < 0.05$; $^{**}P < 0.01$; $^{***}P < 0.001$ (*t*-test).

any timepoint after *Pst* inoculation (Fig. 1b). Thus, DCL1 may play an early role in the induction of defense responses, though its direct impact is uncertain given its extensive function in sRNA biogenesis.

The transcriptomes of mock-, *Pst*-, and *Pst_avrRpt2*-inoculated Arabidopsis were analyzed at multiple time points to investigate transcriptional reprogramming following pathogen infection. Pair-wise comparisons revealed that the number of differentially expressed genes (DEGs) in *Pst_avrRpt2* vs mock and *Pst_avrRpt2* vs *Pst* peaked at 6 hpi, whereas those in *Pst* vs mock peaked at 24 hpi (Supplementary Fig. 1a). Interestingly, most of the upregulated DEGs in *Pst_avrRpt2* vs *Pst* (for simplicity, termed as ETI-DEGs hereafter) at 6 hpi, which mainly belonged to "response to biotic stimulus/stress" (Supplementary Fig. 2), displayed little overlap with those at other timepoints (Supplementary Fig. 1b, c). Another transcriptome study similarly concluded that ETI-DEGs peak at 6 hpi[26]; note that this report used 50% of the inoculum used in our study. Since early ETI-associated responses occur within minutes of inoculation[27], the machinery responsible for ETI-DEG induction presumably functions between these key ETI events.

Whether DCL1-associated sRNAs regulate ETI-induced transcriptional reprogramming was assessed by characterizing nuclear-localized sRNAs (<100 nts) in mock- and *Pst_avrRpt2*-inoculated WT and *dcl1-7* at 1 hpi. Size-distribution analysis showed that, regardless of pathogen inoculation, *dcl1-7* accumulated more RNAs of ≤28 nts, whereas WT accumulated more RNAs of ≥70 nts (Fig. 1c). Additionally, while the nuclear RNA distribution profile was not substantially altered in *dcl1-7* after *Pst_avrRpt2* inoculation, a ~ 2-fold increase in 74 nts and 76/77 nts RNAs was observed in pathogen- vs mock-inoculated WT; a significant increase also was observed in 85/86 nts. Examining >70 nts RNA revealed that many originated from tRNA genes; note that full-length Arabidopsis tRNAs are 71 to 92 nts. Strikingly, tRNA reads in the nuclei of *Pst_avrRpt2*-inoculated WT, but not *dcl1-7*, rose to nearly 10% of the total sRNA population by 1 hpi (Fig. 1d). Dramatic pathogen-induced, DCL1-dependent inductions were observed for a subset of tRNAs (Fig. 1e).

Early rise of DCL1-dependent tRFs in ETI

Since nuclear tRNA levels rose during ETI triggered by *Pst_avrRpt2*, we assessed whether nuclear tsRNAs also increased. Due to tRNA gene redundancy, a sequence-centered analysis, termed MINTmap[19], was used to characterize nuclear tsRNAs of 11 to 40 nts in mock- and *Pst_avrRpt2*-inoculated WT and *dcl1-7* at 1 hpi. Of the four tsRNA classes, 5′-tRFs and 5′-halves predominated; of these, only 5′-tRFs were induced by *Pst_avrRpt2* in a DCL1-dependent manner (Supplementary Fig. 3a). Size distribution analysis of 5′-tRFs revealed peaks at 16 and 31 nt, with the 31 nts tRFs exhibiting DCL1-dependent accumulation after *Pst_avrRpt2* inoculation (Fig. 2a). The 31 nts tRFs were primarily derived from a few tRNAs, with AspGTC predominating (Fig. 2b). The pathogen- and DCL1-dependent accumulation of a 31 nts 5′-tRF derived from $tRNA^{Asp2GTC}$ (designated

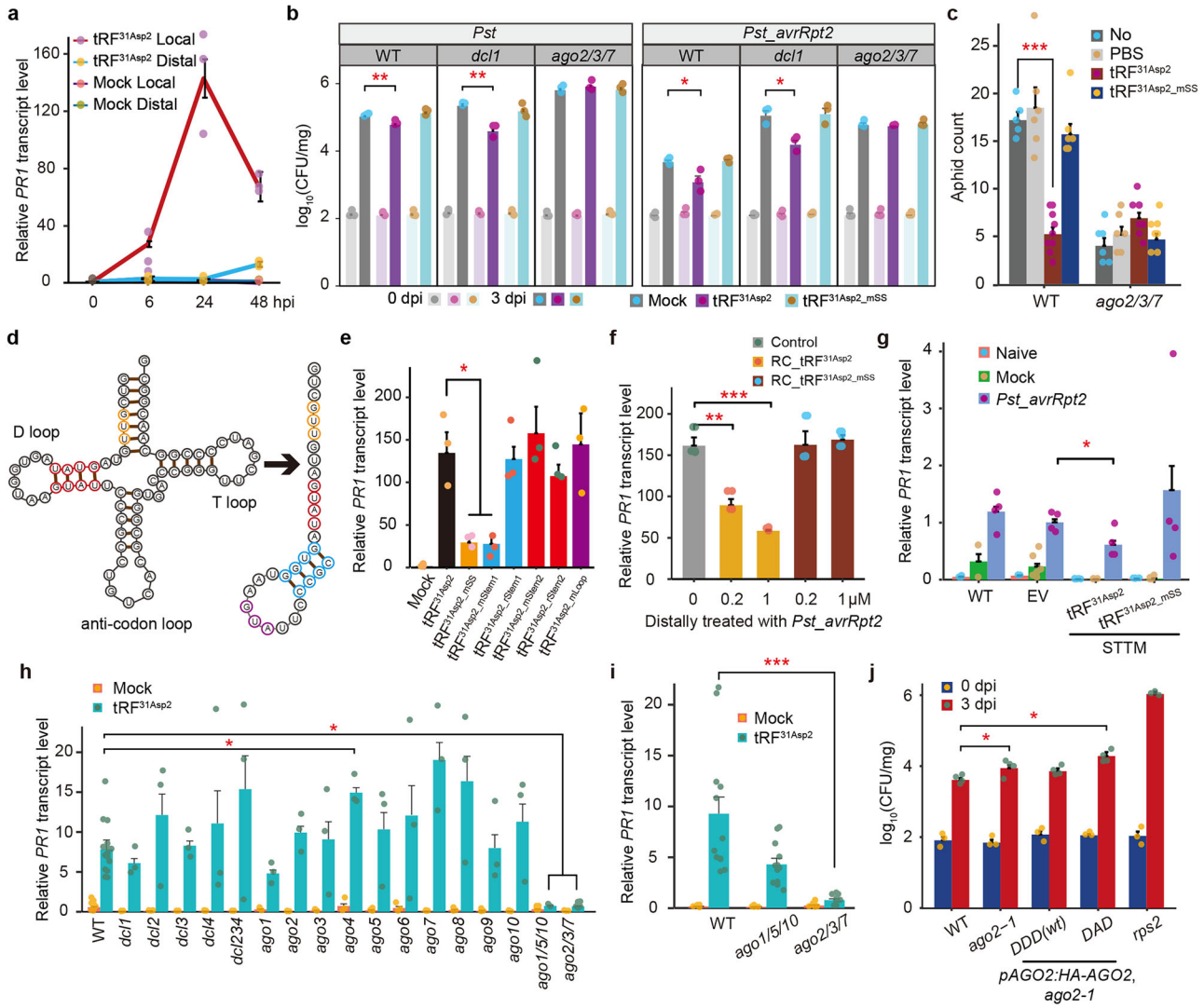

Fig. 3 | tRF^{31Asp2} induces immunity in an AGO2-clade dependent manner. a *PR1* expression in local and distal leaves at the indicated times after tRF^{31Asp2} (1 μM) or buffer infiltration was examined by qRT-PCR. **b** Bacterial growth in WT, *dcl1-7*, and *ago2/3/7* pretreated with tRF^{31Asp2}, tRF^{31Asp2_mSS}, or mock at 0 and 3 dpi with *Pst* and *Pst_avrRpt2*; the mean±RSE ($n = 12$) from three independent experiments is presented. **c** tRF^{31Asp2} promotes enhanced resistance to aphids. The green peach aphid (GPA) numbers at 5 dpi on WT and *ago2/3/7* leaves were pretreated with tRF^{31Asp2}, tRF^{31Asp2_mSS}; untreated (No) and the buffer (PBS)-treated WT used as a control. Plants were initially infested with three adult apterous aphids/plant after 24 hpi. The same experiment was conducted twice with similar results. The mean ± SE ($n = 7$ to 10) is presented. **d** Predicted secondary structure of full-length Asp-2-tRNA^{GTC} and its 31 nt-long 5′-tRF (tRF^{31Asp2}) by RNAfold. **e** *PR1* induction by tRF^{31Asp2} and its mutants at 24 hpi was examined by qRT-PCR; relative transcription levels are presented as the mean ± SD ($n = 3$). Bar colors correspond to target sites in (**d**). **f** Antisense oligonucleotides or buffer were infiltrated into leaves 1 day before distal-infection with *Pst_avrRpt2*; *PR1* was assessed at 1 dpi by qRT-PCR; the mean ± SD ($n = 4$). Three independent experiments were performed with similar results. **g** *PR1* expression in distal leaves of short tandem target mimic (STTM) and empty vector (EV) lines, and WT at 24 hpi with *Pst_avrRpt2* or mock was examined by qRT-PCR; naive is without any treatment; the mean ± SE ($n = 4$). **h**, **i** *PR1* induction in *dcl* and *ago* mutants at 24 hpi responding to 1 (**h**) and 20 (**i**) μM of tRF^{31Asp2} and its mock control. The mean ± SE ($n \geq 4$) is presented. **j** Bacterial growth in WT, *ago2-1*, and *AGO2* complementation lines (DDD and DAD are WT and a slicer mutant, respectively) in *ago2-1* at 0 and 3 day-post-infection (dpi) with *Pst_avrRpt2* with the mean ± SE ($n = 4$); *rps2* is an ETI control. Significance for indicated pairs is noted; $^{*}P < 0.05$; $^{**}P < 0.01$; $^{***}P < 0.001$ (*t*-test except for **c** where Tukey's HSD test was used).

tRF^{31Asp2}) is illustrated in Fig. 2c; this tRF was largely responsible for the increase in AspGTC and generated from cleavage at anticodon stem, which belongs to tRF-5c. This DCL1-dependent increase of tRF^{31Asp2} in response to *Pst_avrRpt2* was also independently confirmed via stem-loop quantitative RT-PCR (Supplementary Fig. 4a) and northern blot analysis (Supplementary Fig. 4b). In addition to *avrRpt2*, other ETI triggering effectors, *avrRpm1* and *avrRps4*, were also found to induce tRF^{31Asp2} comparatively (Supplementary Fig. 4c). We also assessed if DCL1 is directly involved in biogenesis of tRF^{31Asp2} in vitro. Although DCL1 produced the expected 46 nts 5′ end fragment during the processing of pri-miR166g[28], the production of 5′-tRFs at 31 nts by DCL1 was quite limited (indicated by an arrow in Supplementary Fig. 4d). This observation suggests that the reaction may require an extra cofactor to reach its maximum potential.

Reactive oxygen species (ROS), an early molecule elevated during the defense responses, has been shown to increase the level of tsRNAs[18]. Thus, we investigated if the reverse could be true by analyzing the changes in ROS levels following the treatment of tRF^{31Asp2}. While flg22, an epitope derived from a bacterial PAMP flagellin, induced ROS production, both tRF^{31Asp2} and its mutant exhibited no significant elevation over 24 h (Supplementary Fig. 4e, f). This observation suggests that ROS probably acts as an upstream signaling mediator for tsRNAs.

Since AGOs are effector proteins for some tRFs and tRNA-halves[29], the possibility that they interact with nuclear-localized tRFs was assessed. Of the ten Arabidopsis AGOs, AGO1 and AGO2 were selected as they are the most highly expressed in mature leaves[25], and AGO2 was implicated in ETI[8]. Additionally, marginal increases in nuclear-localized AGO2 were noted

following pathogen inoculation (Supplementary Fig. 5). Analysis of the 5′-tRF profile from nuclear-localized AGO1- and AGO2-bound sRNAs, also known as RIP (RNA immunoprecipitation)-seq, in mock-, *Pst*- and *Pst_avrRpt2*-inoculated WT at 1 hpi revealed major peaks at 16 and 31 nts (Fig. 2d). Infection with *Pst_avrRpt2*, but not *Pst*, substantially increased the abundance of AGO1/2-bound 16 nts tRFs and AGO2-bound 31 nts tRFs. Similar to the nuclear tsRNAs (Fig. 2b), AGO2-bound 31 nts tRFs were derived from a subset of tRNAs, with AspGTC predominating (Fig. 2e). Likewise, *Pst_avrRpt2*-induced accumulation of AGO2-associated AspGTC tRFs was largely due to increases in tRF^{31Asp2} (Fig. 2f). A previous RIP-seq of nuclear AGO1 revealed that 21 nts sRNAs starting with 'U' are the major interactors[29]. Consistent with this report, AGO1 associated preferentially with 21 nts sRNAs starting with 'U', whereas AGO2 displayed an elevated association with those with 'A' (Supplementary Fig. 6b). Additionally, when assessing the fold enrichment before and after IP via AGO1/2, larger tRFs (>28 nts) were predominantly enriched (Supplementary Fig. 3c, d). Furthermore, miRNAs known to interact with nuclear AGO1[29] showed specific enrichment in AGO1 IP samples (Supplementary Fig. 3e), confirming the IP specificity. Thus, these findings suggest that some tRFs, including tRF^{31Asp2}, induced by *Pst_avrRpt2* are also associated with AGO2 in the nucleus.

tRF-triggered immunity

Synthetic tRF^{31Asp2} RNA was infiltrated into Arabidopsis leaves to investigate the role of tRF^{31Asp2} in defense responses. tRF^{31Asp2} induced *PR1* expression in a dose-dependent manner (Supplementary Fig. 7a). A time course revealed that *PR1* expression in infiltrated leaves peaked at 24 hpi; an increase in systemic, untreated leaves was observed at 48 hpi (Fig. 3a). We also found that $tRF^{31SerGCT}$ and $tRF^{31ValCAC}$, two 31 nts 5′-tRFs that were not induced by *Pst_avrRpt2*, did not induce *PR1* (Supplementary Fig. 7b). Pretreating WT with tRF^{31Asp2} vs mock led to a ~ 43% reduction in *Pst* growth at 3 dpi while the greater reduction (~75%) was observed in *Pst_avrRpt2* (Fig. 3b). An even greater reduction was observed in tRF^{31Asp2}-pretreated *dcl1-7*, suggesting that tRF^{31Asp2} may be more effective in complementing *dcl1*, which lacks the capability to generate immunity-related tRFs, compared to WT. To expand the analysis, the ability of tRF^{31Asp2} to induce aphid resistance was also tested. Aphid resistance was enhanced significantly in WT pretreated with tRF^{31Asp2} but not buffer. While *ago2/3/7* showed increased resistance to aphids, tRF^{31Asp2} did not provide any additional improvement in resistance (Fig. 3c). This suggests that the aphid resistance induced by tRF^{31Asp2} is dependent on the AGO2 clade. However, we cannot rule out the possibility of additional factors contributing to aphid resistance. It should be noted that miRNA-regulated camalexin by AGO1 was shown to be crucial in aphid resistance[30]. Together, these findings indicate that tRF^{31Asp2} infiltration induces immune responses.

A stem-loop in the tRF structure

tRF^{31Asp2} has a predicted secondary structure with a stem-loop whose location differs from the tRNA D arm (Fig. 3d). We generated synthetic RNAs bearing mutations at four sites (Supplementary Fig. 7c) to characterize which regions of tRF^{31Asp2} are important for biological activity. Additionally, the effect of deleting/adding nts to the 3′ end of tRF^{31Asp2}, based on the sequence of its $tRNA^{Asp2GTC}$, was assessed (Supplementary Fig. 7d). tRF^{31Asp2_mSS} with three altered nts in the 5′ single-strand region (Supplementary Fig. 7b) was substantially less effective at inducing *PR1* expression (Fig. 3e) and immunity against *Pst_avrRpt2*, *Pst* and aphids (Fig. 3b, c). However, the decreased biological activity did not correlate with reduced AGO2 binding, which was comparable in tRF^{31Asp2_mSS} and tRF^{31Asp2} (Supplementary Fig. 7e). tRF^{31Asp2_mStem1}, with mutations disrupting the predicted stem structure, also was compromised for *PR1* induction (Fig. 3e). However, tRF^{31Asp2_rStem1}, containing compensatory mutations restoring the stem structure, induced *PR1* to comparable levels as tRF^{31Asp2}. Mutations in the predicted loop (tRF^{31Asp2_mLoop}) and alterations in tRNA D-loop-associated nts ($tRF^{[31Asp2\_mStem2}$) did not substantially alter *PR1* induction. Adding 4 nts to the 3′ end of tRF^{31Asp2} also did not significantly affect *PR1* induction, whereas trimming 3 or more nts from this end, which impacts the stem-loop structure, abolished *PR1* induction (Supplementary Fig. 7d). Whether an oligonucleotide containing the antisense sequence of tRF^{31Asp2} (RC_tRF^{31Asp2}) could suppress *Pst_avrRpt2*-induced *PR1* expression was assessed. Pretreating leaves with RC_tRF^{31Asp2} prior to infecting lower leaves with *Pst_avrRpt2* suppressed systemic *PR1* expression, whereas $RC\_tRF^{31Asp2\_mSS}$, the antisense sequence of tRF^{31Asp2_mSS}, did not (Fig. 3f). Consistent with this observation, short tandem target mimic (STTM) lines targeting tRF^{31Asp2}, not tRF^{31Asp2_mSS}, displayed reduced systemic *PR1* induction (Fig. 3g). Together, these results suggest that the predicted stem-loop structure and the 5′ sequence of tRF^{31Asp2} are important for its biological activity.

Dependence of tRF^{31Asp2} immunity on the AGO2 clade

We tested whether tRF^{31Asp2} induces immune responses in the *dcl* or *ago* mutant backgrounds. All *dcl* and *ago* single mutants largely exhibited WT-level *PR1* induction, but higher-order mutants defective either for AGO1 or AGO2 clade members (*ago1/5/10* or *ago2/3/7*, respectively) showed significantly lower levels of *PR1* induction (Fig. 3h). Interestingly, when a greater amount of tRF^{31Asp2} was administered to these triple mutants, only *ago2/3/7* failed to induce *PR1* (Fig. 3i). This observation suggests that while the AGO1 clade might be implicated in tRF signaling, the AGO2 clade could plays a relatively more predominent role in this process.

AGO2 requires its catalytic site for target suppression through slicing[31]. We investigated the role of AGO2's slicing catalytic site in its immunity function and found that AGO2 with a slicer mutation (DAD) failed to complement the compromised immune response to *Pst_avrRpt2* in *ago2* (Fig. 3j). Together with the RIP-seq data, these results suggest that loading of tRF^{31Asp2} into AGO2 or its clade members in a catalytically active form could contribute to trigger defense responses.

tRF^{31Asp2}-induced defense genes

To identify tRF^{31Asp2}-induced DEGs, transcriptome analyses were performed (Supplementary Fig. 8a). Comparing the transcriptomes of i) WT treated with tRF^{31Asp2} vs mock, ii) WT treated with tRF^{31Asp2} vs tRF^{31Asp2_mSS}, and iii) WT vs *ago2/3/7* treated with tRF^{31Asp2} identified 810 DEGs present in all three combinations (tRF-DEGs, hereafter) (Supplementary Fig. 8b, c). The majority of these DEGs (503 of 810) also were identified as ETI-DEGs (Supplementary Fig. 8d). These tRF-DEGs mostly belong to "response to stress" such as biotic stimulus (Supplementary Fig. 9). Recent reports revealed that ETI and PTI share a significant number of downstream components[6,7] and identified genes that are unique and overlapping to ETI and PTI[6]. Interestingly, the majority of tRF-DEGs belong to a group in which ETI and PTI are shared (Supplementary Fig. 8e).

Association of tRFs with *Gypsy's* PBS and its homologous sequence in defense genes

We investigated the possibility that tRF^{31Asp2} physically interacts with Arabidopsis chromatin by infiltrating biotinylated tRF^{31Asp2} or tRF^{31Asp2_mSS} into WT and *ago2/3/7* leaves and performing ChAP (Chromatin Affinity Precipitation)-seq analysis. In WT, normalized reads showed that tRF^{31Asp2} interacted with chromatin significantly more than tRF^{31Asp2_mSS}, particularly around the genic area, with these interactions further diminished in *ago2/3/7* mutants (Supplementary Fig. 10a). Using MACS2[32], we identified ChAP-seq peaks by comparing reads from streptavidin beads with those from non-interacting IgG beads. The number of ChAP-seq peaks was significantly reduced in tRF^{31Asp2_mSS} relative to its WT counterpart and again further decreased in *ago2/3/7*, suggesting that the AGO2 clade may facilitate the interaction of tRF^{31Asp2} with chromatin. Interestingly, a considerable number of ChAP-seq peaks were identified within transposon regions (Supplementary Fig. 11a). The greatest number of transposon-localized ChAP-seq peaks that also contained the tRF^{31Asp2} sequence, based on FASTA analysis with an E score of <0.01, were identified in the *Gypsy* and *Copia* superfamilies of long-terminal repeat (LTR)-retrotransposons (Supplementary Fig. 11b). Within the *Gypsy* superfamily, ChAP-seq peaks with the tRF^{31Asp2}

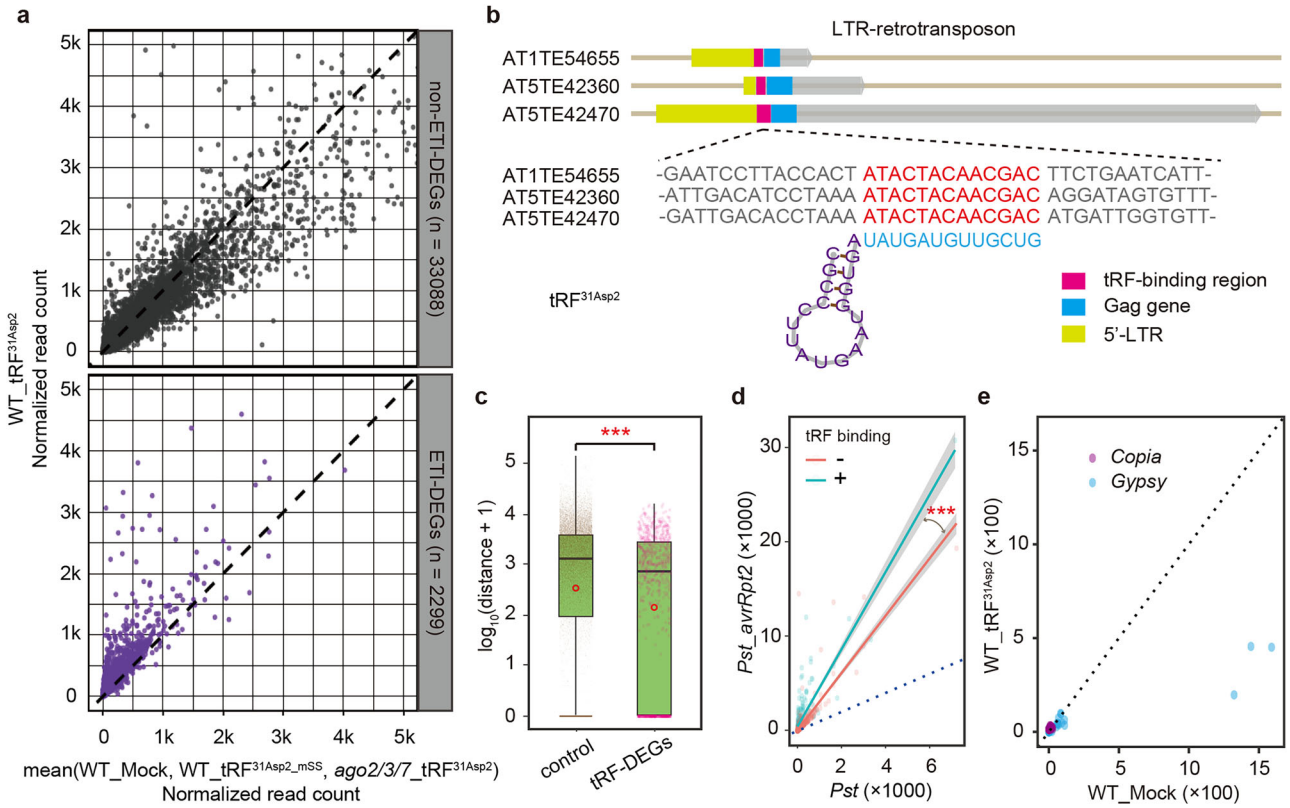

Fig. 4 | tRF^{31Asp2} binds a sequence present in *Gypsy* retrotransposons and nearby ETI-induced genes. a Induction patterns in ETI-DEGs (lower) and non-ETI-DEGs (upper) are shown; the y- and x-axes show normalized read counts from RNA-seq of tRF^{31Asp2}-treated WT, and the mean values of three controls, respectively. **b** The primer binding site of *Gypsy* retrotransposons is highly homologous to tRF^{31Asp2}. **c** Physical distance of tRF-DEGs and control (non-tRF-DEGs) from the nearest tRF^{31Asp2}-binding ChAP-seq peaks. Data are represented as boxplots where the middle line and the dot are respectively the median and the mean, the lower and upper hinges correspond to the first and third quartiles, and the upper/lower whisker extends from the hinge to the largest/smallest value no further than 1.5 × IQR (interquartile range). The y-axis shows the physical distance in bps. Significance for indicated pairs is noted; $^{***}P < 0.001$ (*t*-test). **d** Induction patterns of ETI-DEGs between with and without tRF binding. The y- and x-axes show normalized read counts from *Pst_avrRpt2* and *Pst* at 6 hpi. Significance for indicated slopes is noted; $^{***}P < 10^{-16}$ (Chow test). **e** Induction patterns of transcriptionally active *Copia* and *Gypsy* LTR-retrotransposons. The y- and x-axes show normalized read counts tRF^{31Asp2}-treated WT and its mock control.

sequence were most prevalent in members of *ATGP1* (Supplementary Fig. 11c). Strikingly, the single-stranded 5′ region of tRF^{31Asp2} exhibited perfect complementarity to the *Gypsy* primer binding site (PBS) (Fig. 4b). Binding of *Gypsy* PBS by the 3′ end of tRNAs primes its proliferation[33]. Since the 3′ end of Asp-2-tRNA^{GTC} is complementary to the 5′ sequences of tRF^{31Asp2}, tRF^{31Asp2} might likewise bind these retrotransposons in a sequence-specific manner.

Interestingly, tRF^{31Asp2}-associated peaks were also found in the genic area of many defense-associated genes, including *PR1*, *PR2*, and *PR5*; all the *PR*-associated peaks were statistically significant (Supplementary Fig. 10b), raising an intriguing possibility that this physical interaction could have resulted in the activation of defense genes and immune responses.

Proximity of tRF sites to their DEGs

We speculated that tRF^{31Asp2} might similarly regulate other tRF-DEG expression via interaction with its complementary sequence, which might be located in recognizable or degenerated/unrecognizable transposons; note that transposons are recognized as a critical driver involved in evolving transcriptional networks in plants and animals[34,35]. To assess this possibility, the distance between genes and their nearest ChAP-seq peak was assessed. Interestingly, analysis of ChAP-seq peaks revealed that the peaks were significantly closer to tRF-DEGs (Fig. 4c) than those not, suggesting that defense genes induced by tRF^{31Asp2} may associate with tRF^{31Asp2} itself. We then separately examined ETI-DEGs with and without the tRF overlap. While not all defense genes physically interacted with tRF^{31Asp2}, ETI-DEGs that tRF^{31Asp2} bound exhibited a significantly greater fold induction compared to non-bound counterparts (Fig. 4d). In other words, genes that interact with tRF^{31Asp2} are typically silent under normal conditions but are strongly activated upon defense induction. These findings suggest that tRF^{31Asp2} may function as a transcriptional enhancer, facilitating the expression of otherwise dormant defense genes during ETI.

In contrast to this activating function, some tRFs were shown to suppress retrotransposons[23,24]. We, therefore, examined the changes of transcriptionally active LTR-retrotransposons and found that tRF^{31Asp2} largely suppressed these transposons, particularly *Gypsy* (Fig. 4e). These observations suggest that the tRF binding might be important in inducing neighboring tRF-DEGs while suppressing active retrotransposons.

Discussion

In this study, we have shown that tRF^{31Asp2} is a DCL1-dependent sRNA rapidly induced well before the ETI transcriptomic peak. Treatment of tRF^{31Asp2} alone was sufficient to initiate immune responses robust enough to immunize Arabidopsis against avirulent and virulent *Pst* as well as aphids. The increased resistance exhibited against aphids by tRF^{31Asp2} (Fig. 3c) indicates that this tRF may not be exclusively targeted towards ETI. Recent reports suggest the mutual potentiation between ETI and PTI[6,7]. Interestingly, a majority of tRF-DEGs belonged to a list of genes that are common to both ETI and PTI (Supplementary Fig. 8e), suggesting that tRF^{31Asp2} might play a role in both pathways, although ETI requiring quicker kinetics could be more impacted.

tRF^{31Asp2} bound chromatin at a specific sequence present in *Gypsy* LTR-retrotransposons and defense genes. The abundant presence of tsRNAs and

their likely interacting partners, LTR-retrotransposons, in all plant systems examined[14,35] indicates that the positive regulatory role found herein may be ubiquitous. Although the origin of binding sites in defense genes is uncertain, there is a possibility that these sites are degenerated sequences that originated from LTR-retrotransposons. The analysis supports this speculation that some transcriptional enhancers may have originated from transposons[36]. Interestingly, ETI-DEGs with the tRF^{31Asp2} binding appeared to be induced more steeply (Fig. 4d) than those without, suggesting that this tRF is involved in further accelerating transcriptional induction. RNA activation (RNAa), which is the process of activating transcription through sRNAs, involves the recruitment of RNA polymerase II and associated factors to target genes[37,38]. This is achieved through the binding of 21 nts double-stranded RNAs with mammalian AGO2, which is similar to Arabidopsis AGO1. By interacting with the promoters of target genes, these sRNAs function as enhancers, inducing target genes. Our observations, therefore, suggest that tRF^{31Asp2} may use a similar transcriptional activation mechanism. Consistent with earlier reports[23,24,39], the role of suppressing transposons was also observed for transcriptionally active *Gypsy* LTR-retrotransposons (Fig. 4e). Altering the level of tRFs derived from $tRNA^{GlyGCC}$, another tRF found to be induced by *Pst_avrRpt2* (Fig. 2b, e), was shown to be closely correlated with pancreatic cancer development in mice[40]. Interestingly, tRF^{GlyGCC}, which has the same size as tRF^{31Asp2}, increases in abundance during mouse sperm maturation and has been found to inhibit the endogenous retroelement MERVL and its neighboring genes[24]. Therefore, understanding how these tRFs induce and suppress target genes will be crucial in this emerging tRF biology.

Understanding DCL1's role in immunity (Fig. 1) is complex due to its involvement in generating various miRNAs influencing defense responses[41]. Furthermore, the pleiotropic phenotypes of *dcl1*, affecting growth and flowering[42], further complicate assessing the specific impact of the tRF on defense responses despite its evident involvement in plant immunity when tRF^{31Asp2} triggers robust defense responses (Figs. 3 and 4). Nonetheless, after exposure to *Pst_avrRpt2*, both nuclear tRF^{31Asp2} and its likely precursor, $tRNA^{Asp2GTC}$, exhibited DCL1-dependent increases (Figs. 1e, 2c and Supplementary Fig. 4), suggesting the import of the full-length tRNA and its cleavage to tRFs in the nucleus may depend on DCL1. In addition, the notable presence of tRF^{31Asp2} that did not trigger defense responses prior to pathogen exposure (Fig. 2c and Supplementary Fig. 4) suggests that DCL1 may play a role in generating the defense-activated form of tRF^{31Asp2}. Consistent with this notion, murine Dicer was shown to relocate to the nucleus when exposed to DNA damage[43]. Additionally, human Dicer has been demonstrated to facilitate the nuclear import of a reporter protein by interacting with importins[44]. Notably, tRNAs undergo nuclear import during virus infection or amino acid deprivation in human and yeast cells, known as tRNA retrograde nuclear import[45,46]. Therefore, investigating the potential involvement of DCL1 in the retrograde import of tRNAs presents an intriguing avenue for tRF research.

Finally, our antisense and STTM approaches targeting tRF^{31Asp2} marginally suppress the systemic *PR1* induction (Fig. 3f, g), whereas the delivery of tRF^{31Asp2} significantly induced hundreds of defense genes (Fig. 4a). These findings suggest that there may be additional tRFs involved in assisting defense responses or that these knock-down techniques are inadequate in significantly disrupting defense signaling because of the plentiful presence of other immunity-related tRFs. Nonetheless, the ability to modulate these tRFs to enhance or suppress defense responses indicates that gaining a deeper understanding of these immunity-related tRFs could lead to new biotechnological approaches for managing disease in agriculture.

Methods

Plant materials and growth conditions

Plants were grown in soil at 22 °C, 60% relative humidity, and in a 16 h light period. All Arabidopsis lines used in this study are in the Col-0 background. The following mutant lines were obtained from the Arabidopsis Stock Center or the research groups in indicated references: *ago1-27*[47], *ago2-1* (SALK_003380), *ago3-2* (SALK_005335), *ago4-2*[48], *ago5-1* (SALK_063806), *ago6-3* (SALK_106607), *ago7*[49], *ago8-1* (SALK_139894), *ago9-2* (SALK_112059), *ago10-2* (SALK_047336), *ago2/3/7*[10], *dcl1-7*[50], *dcl2-1* (SALK_064627), *dcl3-1* (SALK_005512), *dcl4-2* (GABI_160G05), *dcl2/3/4* (CS16391), *HA-AGO1*[31], *HA-AGO2*[31] and *HA-AGO2-DAD*[31]. *ago1/5/10* was generated from *ago1-27*, *ago5-1*, and *ago10-2*. *HA-AGO1* (*pAGO1::3HA-AGO1* in *ago1-25*), *HA-AGO2* (*pAGO2::3HA-AGO2* in *ago2-1*) and *HA-AGO2-DAD* (*pAGO2::3HA-AGO2-DAD* in *ago2-1*) lines[51] are transgenic Arabidopsis carrying HA-tagged *AGO1*/*AGO2* under their own promoters. tRF^{31Asp2_STTM} and $tRF^{31Asp2\_mSS\_STTM}$ transgenic Arabidopsis, respectively carrying pFGC5941-PacI-STTM-tRF^{31Asp2_STTM} and pFGC5941-PacI-STTM-$tRF^{31Asp2\_mSS\_STTM}$, were generated as described in ref. 51; oligonucleotides used in the vector constructions are listed in Supplementary Table 1 and Arabidopsis carrying pFGC5941-PacI was used as an empty vector control.

Total and small RNA extraction, semiquantitative/quantitative RT-PCR, and northern blot analysis

Total RNAs were isolated using the TRIzol reagent (Invitrogen). 1 μg of total RNAs were treated by DNase I (NEB), and cDNAs were then synthesized by M-MuLV reverse transcriptase (NEB).

For small RNA preparation, 3.5-week-old WT and *dcl1-7* plants were infiltrated with 10^6 cfu/ml of *Pst* and *Pst_avrRpt2* for 1 hour. After nuclei were isolated as described below, the small RNAs were prepared using the mirVana miRNA Isolation Kit (ThermoFisher).

Real-time quantitative RT-PCR was performed using HOT FIREPol EvaGreen qPCR Mix Plus (Solis BioDyne) with the primers listed in Supplementary Table 1. Relative expression level was calculated from the difference between the threshold cycle (Ct) values of reference and target genes[52]. The reference gene is *Tip41-like* (AT4G34270)[53] for Fig. 1, and *RHIP1* (AT4G26410) for the rest[53].

Stem-loop RT-PCR was performed by following the procedure as described in ref. 54 to assess the levels of tRF^{31Asp2}. Nuclear sRNA served as a template for reverse transcription, using a stem-loop RT primer targeting the six nucleotides at the 3′ end of the tRF. The RT product was amplified using a tRF^{31Asp2}-specific forward primer and a universal reverse primer. Real-time quantitative PCR was performed as described above. Semi-quantitative PCR was conducted using DreamTaq DNA Polymerase (Fisher). *U6*, a small nuclear RNA, was utilized as a reference gene and input control for qPCR and semi-qPCR, respectively[55].

Northern blot procedure was carried out as described in ref. 56 with some modifications. Nucleus was prepared from 5 g of homogenized tissue as described below, and its total RNA was prepared using the *mir*Vana™ miRNA Isolation Kit (Fisher). 175 ng of total RNA was separated on a denaturing 15% polyacrylamide gel. The gel was cut into two parts: the upper part containing larger-sized RNAs was stained with SYBR gold for use as a loading input, while the other part was transferred to a nylon membrane (Roche). Transfer was carried out at 15V for 90 min in a 1x TBE solution at 4 °C. The membrane was cross-linked using 1-ethyl-3-(3-dimethylaminopropyl) carbodiimide (EDC; Sigma). To prepare this, the membrane and saturated Whatman paper were soaked in freshly prepared EDC cross-linking reagent, wrapped in Saran wrap, and incubated at 60 °C for 2 h. Next, residual cross-linking solution was removed by thoroughly rinsing the membrane with ddH_2O and the membrane was placed into hybridization bottle with the RNA side inward. The membrane was pre-hybridized in ULTRAhyb (ThermoFisher) buffer at 55 °C for at least 30 min in hybridization oven. A denatured (95 °C for 1 min) DIG-labeled LNA-DNA probe for tRF^{31Asp2} (5 nM) was hybridized at 55 °C overnight with slow rotation. The hybridized membrane was washed extensively at room temperature using Low Stringent Buffer (twice, 15 min each), High Stringent Buffer (twice, 5 min each) and Washing Buffer (once for 10 min). The membrane was then blocked in Blocking Buffer for 5 hours at room temperature and incubated in an anti-DIG antibody (Roche, 1:15,000) for 45 min. The membrane was washed in DIG Washing buffer four times for 15 min each and incubated in a chemiluminescence substrate, CSPD

(Roche), for 5 min in a room temperature, followed by dark incubation at 37 °C for 15 min. The presence of tRF was detected by imaging using an Azure imaging station.

Nucleus enrichment

Nucleus-enriched and -depleted fractions were prepared as previously described in ref. 57 with the following modifications. Around 1 g leaves were homogenized in liquid N2 using pre-chilled mortar and pestle followed by homogenization in 5 mL of NIB [250 mM sucrose (Sigma), 10 mM NaCl (ThermoFisher), 15 mM PIPES pH 6.8 (ThermoFisher), 0.8% Triton X-100 (Sigma) and 0.1 mM PMSF (Sigma)] with 1x Protease Inhibitor Cocktail (ThermoFisher) at 4 °C. This extract was centrifuged at 300 x g for 5 min at 4 °C to remove the debris and filtered through a double layer of Miracloth (Sigma). Nuclei-enriched fraction was obtained by centrifuging at 1500 x g for 10 min; its supernatant was nucleus-depleted fraction. For the nucleus-depleted fraction, the supernatant was centrifuged again at 1500 x g for 5 min and 200 µL of the supernatant was collected in a new Eppendorf tube. For the nuclei-enriched fraction, the pellet was washed 3–4 times at 1500 x g for 2 min to remove any residual green color. Both the nuclei-enriched and depleted fractions were mixed with 4x SDS sample preparation buffer for western blot. Immunoblotting (IB) analysis with α-HA (1:5000) (Novus) was performed to track the AGO proteins; α-phosphoenolpyruvate carboxylase antibody (α-PEPC, 1:25,000) (Rockland) and α-histone H3 antibody (1:25,000) (Abcam) were used to ensure depletion and enrichment of nuclei, respectively.

IB (immunoblot) and AB (affinityblot) analysis

IB and AB blot analyses were performed as described in ref. 58. For IB, transferred proteins on PVDF (ThermoFisher) membrane were probed with indicated antibodies at 4 °C for 12 h. For AB, transferred tRF^{31Asp2} and tRF^{31Asp2_mSS} oligos on Hybond-N+ membrane (ThermoFisher) were probed with α-streptavidin-HRP (ThermoFisher) at 4 °C for 12 h. For AB, separated biotin labeled tRF^{31Asp2} and tRF^{31Asp2_mSS} oligos using 15% Urea-PAGE were transferred on Hybond-N+ membrane (ThermoFisher) then, probed with α-streptavidin-HRP (ThermoFisher) at 4 °C for 12 h. These blots were visualized via chemiluminescence using ECL2 (ThermoFisher).

Quantification of bands on images

The band intensities in IB/northern blots and stem-loop semiquantitative PCR were quantified using ImageJ[59]. Mean grey values of the target and loading input bands were calculated by subtracting the background. For the northern blot and the stem-loop semiquantitative PCR, the band intensity ratio of α-DIG/SYBR gold and tRF^{31Asp2}/*U6* was presented, respectively. For IB blot, mean grey values for both α-HA and α-H3 were separately calculated, and the ratio of α-HA/α-H3 was presented.

Pathogen infection assay

3.5-week-old Arabidopsis plants were used for the resistance assay. Three leaves of each plant were syringe-infiltrated from the abaxial side with a suspension of *Pst_avrRpt2* or *Pst* at 10^5 cfu/ml. Bacterial growth was determined at 0- and 3-days post-infection (dpi) as described in ref. 25. *Pst* along with its avirulent strain carrying the effectors *avrRpt2* (*Pst_avrRpt2*), was cultured overnight at 28 °C in King's B medium (10 g protease peptone, 0.75 g K_2HPO_4, 10 ml 50% glycerol per 500 ml), supplemented with 2 mM $MgSO_4$ and appropriate antibiotics (50 µg/ml rifamycin or kanamycin). Leaves from 3.5-week-old plants were hand-inoculated with bacterial suspensions at a concentration of 10^5 cfu/ml using a needleless syringe. To measure *in planta* bacterial growth, two leaves were collected as a set, weighed, and ground in 500 µl of ddH_2O. Serial dilutions of the homogenate were plated on LB medium containing 50 µg/ml kanamycin. The plates were incubated at 28 °C, and bacterial colony-forming units (cfu) were counted at 0 and 3 days post-inoculation.

Nucleotide Infiltration

RNA and DNA oligos delivered to 3.5-week-old Arabidopsis leaves are listed in Supplementary Table 1. These oligos in 1x PBS were denatured at 95 °C for a few seconds and renatured by gradually cooling to 25 °C at 5 °C/min. Renatured nucleotides were syringe-infiltrated into the abaxial side of the leaves. Delivery of a tRF RNA nucleotide into the nucleus was initially confirmed by using a 5′ 6-fluorescein (FAM)-conjugated one as shown in Supplementary Fig. 12; sRNAs were extracted from the nucleus-enriched fraction of WT plants infiltrated with FAM-conjugated tRF^{44Asp2} oligo, as described above, and visualized by SYBR gold staining for general RNAs and FAM-specific fluorescence scanning in Typhoon FLA 9000 (GE) for FAM-oligos.

Treatment of the antisense nucleotides on leaves distally infected by *Pst_avrRpt2*

Three leaves were infected with *Pst_avrRpt2* at 10^7 cfu/ml for one day. Uninfected leaves were then treated with 0.2 and 1 µM of RC_tRF^{31Asp2} and $RC\_tRF^{31Asp2\_mSS}$ oligos, respectively, for 24 h; 1x PBS buffer was used as a negative control.

Plant immunization assay

Leaves of 3.5-week-old Arabidopsis plants were infiltrated with 1 µM of tRF^{31Asp2} or tRF^{31Asp2_mSS} oligos for one day. The same leaves were then infected with *Pst* and *Pst_avrRpt2* at 10^5 cfu/ml. Bacterial growth was determined at 0 and 3 dpi.

Aphid propagation and bioassay

The green peach aphid (GPA) colony was reared as previously described in ref. 60. Briefly, the GPA was reared on an equal mixture of commercially available radish (*Raphanus sativus*) and mustard (*Brassica juncea*) plants (Main Street Seed & Supply) in a Percival growth chamber with a 14 h/10 h (light/dark) photoperiod, 160 µE m^{-2} s^{-1}, 22 °C, and 50% to 60% relative humidity. Three-week-old Arabidopsis WT and *ago2/3/7* plants were used for aphid bioassays. Plants were infiltrated with the tRF nucleotides as described above. Three adult apterous GPAs were placed in a 1.5 cm diameter clip cage on leaves one dpi with tRF^{31Asp2} or tRF^{31Asp2_mSS}. The total numbers of GPAs (adults + nymphs) were counted after five days. Statistical analysis was performed using PROC GLIMMIX in SAS 9.3 (SAS Institute) and multiple comparison analyses were carried out using Tukey's HSD test.

In vitro transcription and labeling of RNA, and DCL1 processing assay

A pre-$tRNA^{Asp2}$ (AT5G59055) was amplified using pT7-tRNA_AspGTC_F and tRNA_AspGTC_R primers and cloned into pJET1.2 (Fisher). This plasmid was used to synthesize an amplicon by PCR with pT7- F and tRNA_AspGTC_R primers, which was used for generating a pre-$tRNA^{Asp2GTC}$ in vitro using the HiScribe T7 high-yield RNA synthesis kit (NEB). The pre-$tRNA^{Asp2GTC}$ was treated with DNase I and calf intestinal alkaline phosphatase, labeled with $^{\gamma-32P}$ATP using T4 polynucleotide kinase (PNK), and gel-purified.

Recombinant DCL1 (0.05 pmol), HYL1 (0.1 pmol), SE (0.1 pmol) and RNA substrates at 500 counts per minute after PNK labeling were added to 20 µl assay buffer containing 20 mM Tris-HCl/7.5, 50 mM KCl, 4 mM $MgCl_2$, 1 mM DTT, 5 mM ATP, 5 mM GTP and 1 U/µl Superase-In RNase Inhibitor (ThermoFisher). The final pooled concentration of NaCl and KCl was ~70 mM, of which ~20 mM salt was from protein dialysis buffer and RNA-dissolved buffer. The reconstitution assay was carried out at 37 °C for 1 hr. The reactions were stopped by adding 1 volume TBE-Urea sample buffer (8 M Urea, 2 mM Tris-HCl/7.5, 20 mM EDTA, bromophenol blue/xylene cyanol), being heated at 95 °C for 10 min and then being chilled on ice. The reactions were loaded into 10% denaturing polyacrylamide gel and visualized with a phosphor imaging plate (GE Healthcare).

mRNA-Sequencing library preparation

For antibacterial transcriptome analysis, 3.5-week-old Arabidopsis WT leaves were collected at 0, 1, 6, 24 and 48 hpi with *Pst_avrRpt2* or *Pst* at 10^6 cfu/ml was used to generate Illumina-compatible sequencing libraries. 1 µg of mRNAs enriched by Poly(A) Magnetic Isolation Module (NEB) were reverse-transcribed, end-repaired, and adapter-ligated via NEBNext Ultra II RNA Library Prep Kit for Illumina (NEB). These libraries were sequenced using an Illumina HiSeq 4000 at the University of Texas at Austin Genomic Sequencing and Analysis Facility.

For RNA-seq with tRF, 1 µM of tRF^{31Asp2} and tRF^{31Asp2_mSS} oligos were infiltrated into 3.5-week-old WT and *ago2/3/7* plants for one day, and their RNAs were extracted as described above. A paired-end sequencing was run using BGISEQ-500 with a read length of 100 bp (BGI, Shenzhen, China).

sRNA-Sequencing library preparation

The nuclear sRNAs were treated by 10 U of T4 polynucleotide kinase (NEB) at 37 °C for 40 min to remove cyclic phosphate at the 3′ end. Small RNA libraries were prepared by the QIAseq miRNA Library Kit for Illumina (Qiagen) following manufacturer protocol. A single-end sequencing was run by using BGISEQ-500 with a read length of 100 bp (BGI, Shenzhen, China).

RIP-Sequencing library preparation

10^6 cfu/ml of *Pst* DC3000 with and without *avrRpt2* was infiltrated into 3.5-week-old *HA-AGO1*, *HA-AGO2* lines for 1 h; WT plants were used as a negative control. Around 10 g of leaf tissue was crosslinked in 1% formaldehyde at room temperature for 20 min and ground with liquid N_2. Nuclei extract prepared as described above were co-immunoprecipitated with α-HA-conjugated gel (Sigma). Immunoprecipitated HA-AGO1 and HA-AGO2 proteins were eluted using HA peptides (GenScript). After reverse-crosslinking and digestion by proteinase K (NEB), purified sRNAs were subjected to sRNA-seq library preparation following the protocol described above. sRNAs purified from input fractions before co-IP with α-HA were used as an input control. sRNA-seq libraries were sequenced on an Illumina MiSeq in 2 × 100 bp paired-end mode except for the input control, using DNBSEQ-G400 with a read length of 2 × 100 bp paired-end mode (BGI, Shenzhen, China).

Chromatin-affinity precipitation (ChAP)-Sequencing

Biotin-labeled tRF^{31Asp2} and tRF^{31Asp2_mSS} at 5 nmole were infiltrated into 3.5-week-old WT and *ago2/3/7* plants for 1 h; uninfiltrated WT plants were used as controls. ChAP was performed as described[61] with the following minor modifications. Collected tissues were crosslinked with 1% formaldehyde at room temperature for 15 min and ground with liquid N_2. Nuclei isolated as described above were lysed in the lysis buffer (50 mM HEPES pH 7.5, 140 mM NaCl, 2 mM EDTA, 1% Triton X-100, 0.1% SDS and 25 U/ml RNase Inhibitor) and sonicated (Diagenode, Bioruptor Pico) for the 10 cycles of 30 s on/off interval. Biotin-bound DNA was affinity-purified from nuclear lysate using Dynabeads M-280 streptavidin (ThermoFisher) overnight at 4 °C. As a negative control, DNA was pulled down using MagnaBind Goat Anti-Rabbit IgG (Fisher). After reverse cross-linking and digestion by proteinase K (NEB), DNAs were recovered and used for the ChAP-seq library using NEBNext Ultra II DNA Library Prep kit (NEB). Pair-end sequencing was performed using BGISEQ-500 with a read length of 100 bp (BGI, Shenzhen, China).

ROS measurement

Leaf discs (5-mm diameter) from 3.5-week-old soil-grown Arabidopsis plants were incubated overnight with water in 96-well plates to eliminate the wounding effect. ROS burst was measured by a luminol-based assay as described[62] in the presence of tRF^{31Asp2} (1 µM), tRF^{31Asp2_mSS} (1 µM), flg22 (0.1 µM), or water by using Synergy H1 plate reader (Biotek).

RNA-seq data analysis

Reads from RNA-seq of *Pst* treatment were trimmed for the adapter (AGATCGGAAGAGCACACGTCTGAACTCCAGTCAC) via cutadapt (v2.10)[63]. The adapters of raw reads were also trimmed for RNA-seq of tRF treatment by BGI-Genomics. The clean reads were aligned to the *Arabidopsis* genome (Araport11)[64] using HISAT2 (v2.1.0)[65]. Beyond the default parameters for RNA-seq of *Pst* treatment, the paired-end alignment options were set '--no-mixed, --no-discordant' in the case of tRF-RNA-seq. Alignment results were sorted using samtools (v1.10)[66] and fed into HT-seq (v0.13.5)[67] for read counting. The read coverage tables produced by HT-seq were fed into DESeq2[68] to generate a normalized expression table using DESeq2's median of ratios normalization method. Principal component analysis (PCA) was performed using "prcomp" implemented in R. The differentially expressed genes (DEGs) were then identified following the pipelines of DESeq2. For RNA-seq of *Pst* treatment, DEGs were identified using *Pst_avrRpt2* and *Pst* as the numerator and the denominator, respectively. Upregulated DEGs were identified using a p-adjusted value less than or equal to 0.01 with a $\log_2$ fold change greater than 1. For RNA-seq of tRF, three sets of DEGs (p-adjusted value ≤ 0.05; log2 fold-change ≥ 1) were identified using WT treated with tRF^{31Asp2} as the numerator and the following three controls as denominators: WT treated with mock, WT treated with tRF^{31Asp2_mSS}, and *ago2/3/7* treated with tRF^{31Asp2}. Upregulated tRF-DEGs were identified from the common set of all three DEGs identified from the three comparisons described above.

Analysis of tRNAs, tRFs, and tRNA-halves in sRNA and RIP sequence datasets

Reads from nuclear sRNA-seq and RIP-seq were trimmed of adapter sequences (AACTGTAGGCACC) via cutadapt (v2.10). We used 642 Arabidopsis nuclear tRNA genes annotated in GtRNAdb2[69]. For analyzing the presence of tRNAs in reads larger than 70 nts, Bowtie2 (v2.2.9)[70] was used to map reads to the tRNA sequences using the option '--no-unal'. The tRNA-aligned read counts were generated for each tRNA isoacceptor and size.

For the tRFs and tRNA-halves analysis, reads were mapped using MINTmap software[19]. Each tRF and tRNA-half sequence was grouped based on sequence, tRNA isoacceptor, tRF type, and length, as per MINTmap annotation. Normalized counts (RPM) were generated by using total reads as a denominator. Ambiguous alignments that can also align with non-tRNA sequences were removed from the analysis. Over 98% of tRF reads were tRNA-exclusive alignments.

For the fold-of-enrichment analysis, reads from input samples were mapped and normalized using MINTmap software[19], as described above. The fold-of-enrichment was then calculated by dividing the normalized values of the post-IP samples by those of the input samples.

ChAP-seq data analysis

Pair-end reads were adapter-trimmed (forward: GATCGGAAGAGCACACGTCTGAACT, reverse: GATCGGAAGAGCGTCGTGTA) and quality-trimmed (3:25) via cutadapt (v2.10) and trimmomatic (v0.36), respectively. Trimmed reads were aligned to the Arabidopsis genome (Araport 11)[64] using Bowtie2 (v2.2.9)[70] with the options '--no-unal, --no-discordant, --end-to-end, --no-mixed'. Only unique alignments aligned to the nuclear genome were retained. Peaks were identified by MACS2[71] with default parameters, and filtered with q-value ≤ 0.05 using aligned reads between biotin-binding streptavidin beads and non-targeted IgG beads for tRF^{31Asp2} and tRF^{31Asp2_mSS}. Four biologically independent batches were separately analyzed to call peaks that associated significantly with tRF^{31Asp2} and tRF^{31Asp2_mSS}, relative to the non-targeted control. Reproducible peaks found in a minimum of two independent biological replicates were merged as primary peaks.

We investigated the relationship between these primary peaks and transposons (TEs). The annotation of TEs was based on Araport11 updated on March 2021[64]. TEs shorter than 1000 bp were excluded from the analysis. First, we analyzed the classification of (TEs) that overlapped

with the primary ChAP-peaks. The search for sequence similarity between tRF^{31Asp2} and the peaks was performed using FASTA with the option 'U' for tRF^{31Asp2}, allowing an RNA-DNA alignment. The peaks carrying significantly homologous sequences (E score of 0.05 or lower) were further analyzed for the classification of overlapping TEs. In addition, we also explored the long terminal repeat retrotransposons (LTR-RTs) associated with the tRF^{31Asp2} binding sites. The LTR-RTs were identified using both LTRharvest[72] and LTRfinder[73], and filtered following the LTR_retriever pipeline[74]. The potential tRF^{31Asp2} binding sites were analyzed for the LTR-RTs that overlapped with ChAP-peaks. Only the LTR-RTs with significant tRF^{31Asp2} binding sequences located between the 5′-LTR and *GAG* gene were retained for sequence alignment among LTR-RTs and tRF^{31Asp2}.

We surveyed the relationship between genes and ChAP-peaks. The ChAP-seq reads mapped within gene body and upstream/downstream regions were calculated and normalized (RP10M) within 10 bp windows around the TSS (transcription starting site) and TTS (transcription termination site) of tRF-DEGs identified as described above. All of the four batches were merged together. The physical distances between genes and ChAP-peaks were calculated using bedtools (v2.26.0) of the closest distance between tRF^{31Asp2} binding sites and genes were made for TE and non-TE associated tRF^{31Asp2} binding sites, as well as tRF-DEGs and non-tRF-DEGs, respectively.

Sequence homology, RNAfold and 5′ terminal nucleotides analysis

FASTA (v36.3)[75] was used to obtain an E-value (the number of expected hits of similar quality found just by chance) in sequence homology to 13 nts of 5′ single-strand sequence of tRF^{31Asp2}. The tRF sequence was aligned to ChAP-peak sequences identified above with the option '-U' allowing an RNA-DNA alignment.

RNAfold[76] was used to predict secondary structures of tRNA and its fragments with the default parameters.

Trimmed reads in 21 nts were aligned to the TAIR10 reference genome using Bowtie2 (v2.2.9)[70]. Subsequently, reads aligned to rRNA, tRNA, snRNA, and snoRNA were eliminated using samtools (v1.10)[66]. Then, 21 nts reads mapping to miRNA and siRNA after excluding those present in the WT control were analyzed for the 5′ terminal nucleotide.

Reagent details

Detailed information on the reagents used in this study, including vendor names and catalog numbers, is provided in Supplementary Table 2.

Statistics and Reproducibility

For statistical analysis, unpaired Student's t-tests or unpaired One-way ANOVA with Tukey post hoc tests were used to compare two different conditions. The following values were used: $^{***}p < 0.001$; $^{**}p < 0.01$; $^{*}p < 0.05$. GO enrichment analysis was performed using goProfiles[77] to identify significantly enriched GO categories. Only GO categories with a false discovery rate (FDR) of less than 0.01 were considered significant and are presented in the results. The Wilcoxon rank sum test was employed to compare the expression levels of the *PR1/2/5* genes between different treatment groups. This non-parametric test was selected to assess differences in gene expression without assuming a normal distribution of the data. Fisher's LSD post-hoc test was conducted to determine which specific groups (non-TE or TE) showed significant differences after the initial ANOVA analysis indicated overall group differences. The significance level was set at $p < 0.05$. The n value, ranging from 2 to 12, was provided to indicate the number of samples or independent experiments. All experiments were independently reproduced with similar outcomes.

Reporting summary

Further information on research design is available in the Nature Portfolio Reporting Summary linked to this article.

Data availability

Deep-sequencing data have been deposited in the SRA database and processed data from the ChAP-seq (bed alignment files, bw genome browser files, and narrowPeak peak-calling files) have been deposited to the GEO database. These SRA and GEO data are accessible through BioProject number PRJNA788635 whose processed data at the final step are provided as Supplementary Data 1–6. All the data, the main text, or the supplementary materials are available from the corresponding author on request. Numerical source data for all graphs in the manuscript can be found in Supplementary Data 7. Uncropped images are presented in Supplementary Fig. 13.

Code availability

No custom computer code or algorithm was used in this study.

Received: 2 December 2024; Accepted: 13 February 2025;
Published online: 01 April 2025

References

1. Toruno, T. Y., Stergiopoulos, I. & Coaker, G. Plant-Pathogen Effectors: Cellular Probes Interfering with Plant Defenses in Spatial and Temporal Manners. *Annu Rev. Phytopathol.* **54**, 419–441 (2016).
2. Jones, J. D. & Dangl, J. L. The plant immune system. *Nature* **444**, 323–329 (2006).
3. Jubic, L. M., Saile, S., Furzer, O. J., El Kasmi, F. & Dangl, J. L. Help wanted: helper NLRs and plant immune responses. *Curr. Opin. Plant Biol.* **50**, 82–94 (2019).
4. Tsuda, K., Sato, M., Stoddard, T., Glazebrook, J. & Katagiri, F. Network properties of robust immunity in plants. *PLoS Genet* **5**, e1000772 (2009).
5. Tsuda, K. & Somssich, I. E. Transcriptional networks in plant immunity. *N. Phytol.* **206**, 932–947 (2015).
6. Yuan, M. et al. Pattern-recognition receptors are required for NLR-mediated plant immunity. *Nature* **592**, 105–109 (2021).
7. Ngou, B. P. M., Ahn, H. K., Ding, P. & Jones, J. D. G. Mutual potentiation of plant immunity by cell-surface and intracellular receptors. *Nature* **592**, 110–115 (2021).
8. Bologna, N. G. & Voinnet, O. The diversity, biogenesis, and activities of endogenous silencing small RNAs in Arabidopsis. *Annu Rev. Plant Biol.* **65**, 473–503 (2014).
9. Vaucheret, H. Plant ARGONAUTES. *Trends Plant Sci.* **13**, 350–358 (2008).
10. Zhang, X. et al. Arabidopsis Argonaute 2 regulates innate immunity via miRNA393(*)-mediated silencing of a Golgi-localized SNARE gene, MEMB12. *Mol. Cell.* **42**, 356–366 (2011).
11. Jimeno, S., Balestra, F. R. & Huertas, P. The Emerging Role of RNA Modifications in DNA Double-Strand Break Repair. *Front Mol. Biosci.* **8**, 664872 (2021).
12. Su, Z., Wilson, B., Kumar, P. & Dutta, A. Noncanonical Roles of tRNAs: tRNA Fragments and Beyond. *Annu Rev. Genet* **54**, 47–69 (2020).
13. Ramirez, V. et al. A 2'-O-Methyltransferase Responsible for Transfer RNA Anticodon Modification Is Pivotal for Resistance to Pseudomonas syringae DC3000 in Arabidopsis. *Mol. Plant Microbe Interact.* **31**, 1323–1336 (2018).
14. Fangfang, J. & Zhigang, G. Emerging role of a novel small non-coding regulatory RNA: tRNA-derived small RNA. *ExRNA* **1**, 39 (2019).
15. Kumar, P., Anaya, J., Mudunuri, S. B. & Dutta, A. Meta-analysis of tRNA derived RNA fragments reveals that they are evolutionarily conserved and associate with AGO proteins to recognize specific RNA targets. *BMC Biol.* **12**, 78 (2014).
16. Fu, H. et al. Stress induces tRNA cleavage by angiogenin in mammalian cells. *FEBS Lett.* **583**, 437–442 (2009).
17. Levitz, R. et al. The optional E. coli prr locus encodes a latent form of phage T4-induced anticodon nuclease. *EMBO J.* **9**, 1383–1389 (1990).

18. Thompson, D. M. & Parker, R. The RNase Rny1p cleaves tRNAs and promotes cell death during oxidative stress in Saccharomyces cerevisiae. *J. Cell Biol.* **185**, 43–50 (2009).
19. Loher, P., Telonis, A. G. & Rigoutsos, I. MINTmap: fast and exhaustive profiling of nuclear and mitochondrial tRNA fragments from short RNA-seq data. *Sci. Rep.* **7**, 41184 (2017).
20. Hou, J., Li, Q., Wang, J. & Lu, W. tRFs and tRNA Halves: Novel Cellular Defenders in Multiple Biological Processes. *Curr. Issues Mol. Biol.* **44**, 5949–5962 (2022).
21. Kuscu, C. et al. tRNA fragments (tRFs) guide Ago to regulate gene expression post-transcriptionally in a Dicer-independent manner. *RNA* **24**, 1093–1105 (2018).
22. Ren, B., Wang, X., Duan, J. & Ma, J. Rhizobial tRNA-derived small RNAs are signal molecules regulating plant nodulation. *Science* **365**, 919–922 (2019).
23. Schorn, A. J., Gutbrod, M. J., LeBlanc, C. & Martienssen, R. LTR-Retrotransposon Control by tRNA-Derived Small RNAs. *Cell* **170**, 61–71.e11 (2017).
24. Sharma, U. et al. Biogenesis and function of tRNA fragments during sperm maturation and fertilization in mammals. *Science* **351**, 391–396 (2016).
25. Pujara, D. S. et al. Imaging-based resistance assay using enhanced luminescence-tagged Pseudomonas syringae reveals a complex epigenetic network in plant defense signaling pathways. *Mol Plant Microbe Interact* **34**, 990–1000 (2021).
26. Mine, A. et al. The Defense Phytohormone Signaling Network Enables Rapid, High-Amplitude Transcriptional Reprogramming during Effector-Triggered Immunity. *Plant Cell* **30**, 1199–1219 (2018).
27. Cui, H., Tsuda, K. & Parker, J. E. Effector-triggered immunity: from pathogen perception to robust defense. *Annu Rev. Plant Biol.* **66**, 487–511 (2015).
28. Zhu, H. et al. Bidirectional processing of pri-miRNAs with branched terminal loops by Arabidopsis Dicer-like1. *Nat. Struct. Mol. Biol.* **20**, 1106–1115 (2013).
29. Liu, C. et al. Arabidopsis ARGONAUTE 1 Binds Chromatin to Promote Gene Transcription in Response to Hormones and Stresses. *Dev. Cell* **44**, 348–361.e347 (2018).
30. Kettles, G. J., Drurey, C., Schoonbeek, H. J., Maule, A. J. & Hogenhout, S. A. Resistance of Arabidopsis thaliana to the green peach aphid, Myzus persicae, involves camalexin and is regulated by microRNAs. *N. Phytol.* **198**, 1178–1190 (2013).
31. Carbonell, A. et al. Functional analysis of three Arabidopsis ARGONAUTES using slicer-defective mutants. *Plant Cell* **24**, 3613–3629 (2012).
32. Liu, T. Use model-based Analysis of ChIP-Seq (MACS) to analyze short reads generated by sequencing protein-DNA interactions in embryonic stem cells. *Methods Mol. Biol.* **1150**, 81–95 (2014).
33. Schorn, A. J. & Martienssen, R. Tie-Break: Host and Retrotransposons Play tRNA. *Trends Cell Biol.* **28**, 793–806 (2018).
34. Cordaux, R. & Batzer, M. A. The impact of retrotransposons on human genome evolution. *Nat. Rev. Genet* **10**, 691–703 (2009).
35. Galindo-Gonzalez, L., Mhiri, C., Deyholos, M. K. & Grandbastien, M. A. LTR-retrotransposons in plants: Engines of evolution. *Gene* **626**, 14–25 (2017).
36. Judd, J., Sanderson, H. & Feschotte, C. Evolution of mouse circadian enhancers from transposable elements. *Genome Biol.* **22**, 193 (2021).
37. Kwok, A., Raulf, N. & Habib, N. Developing small activating RNA as a therapeutic: current challenges and promises. *Ther. Deliv.* **10**, 151–164 (2019).
38. Li, L. C. et al. Small dsRNAs induce transcriptional activation in human cells. *Proc. Natl. Acad. Sci. USA* **103**, 17337–17342 (2006).
39. Martinez, G., Choudury, S. G. & Slotkin, R. K. tRNA-derived small RNAs target transposable element transcripts. *Nucleic Acids Res*. **45**, 5142–5152 (2017).
40. Pan, L. et al. Inflammatory cytokine-regulated tRNA-derived fragment tRF-21 suppresses pancreatic ductal adenocarcinoma progression. *J. Clin. Invest.* **131** https://doi.org/10.1172/JCI148130 (2021).
41. Qiao, Y. et al. Small RNAs in Plant Immunity and Virulence of Filamentous Pathogens. *Annu Rev. Phytopathol.* **59**, 265–288 (2021).
42. Schauer, S. E., Jacobsen, S. E., Meinke, D. W. & Ray, A. DICER-LIKE1: blind men and elephants in Arabidopsis development. *Trends Plant Sci.* **7**, 487–491 (2002).
43. Burger, K. & Gullerova, M. Nuclear re-localization of Dicer in primary mouse embryonic fibroblast nuclei following DNA damage. *PLoS Genet* **14**, e1007151 (2018).
44. Doyle, M. et al. The double-stranded RNA binding domain of human Dicer functions as a nuclear localization signal. *RNA* **19**, 1238–1252 (2013).
45. Zaitseva, L., Myers, R. & Fassati, A. tRNAs promote nuclear import of HIV-1 intracellular reverse transcription complexes. *PLoS Biol.* **4**, e332 (2006).
46. Kramer, E. B. & Hopper, A. K. Retrograde transfer RNA nuclear import provides a new level of tRNA quality control in Saccharomyces cerevisiae. *Proc. Natl. Acad. Sci. USA* **110**, 21042–21047 (2013).
47. Morel, J. B. et al. Fertile hypomorphic ARGONAUTE (ago1) mutants impaired in post-transcriptional gene silencing and virus resistance. *Plant cell* **14**, 629–639 (2002).
48. Agorio, A. & Vera, P. ARGONAUTE4 is required for resistance to Pseudomonas syringae in Arabidopsis. *Plant Cell* **19**, 3778–3790 (2007).
49. Montgomery, T. A. et al. Specificity of ARGONAUTE7-miR390 interaction and dual functionality in TAS3 trans-acting siRNA formation. *Cell* **133**, 128–141 (2008).
50. Lang, J. D., Ray, S. & Ray, A. sin 1, a mutation affecting female fertility in Arabidopsis, interacts with mod 1, its recessive modifier. *Genetics* **137**, 1101–1110 (1994).
51. Tang, G. et al. Construction of short tandem target mimic (STTM) to block the functions of plant and animal microRNAs. *Methods* **58**, 118–125 (2012).
52. Schmittgen, T. D. & Livak, K. J. Analyzing real-time PCR data by the comparative C(T) method. *Nat. Protoc.* **3**, 1101–1108 (2008).
53. Hong, S. M., Bahn, S. C., Lyu, A., Jung, H. S. & Ahn, J. H. Identification and testing of superior reference genes for a starting pool of transcript normalization in Arabidopsis. *Plant Cell Physiol.* **51**, 1694–1706 (2010).
54. Varkonyi-Gasic, E. Stem-Loop qRT-PCR for the Detection of Plant microRNAs. *Methods Mol. Biol.* **1456**, 163–175 (2017).
55. Matoušková, P. et al. Reference genes for real-time PCR quantification of messenger RNAs and microRNAs in mouse model of obesity. *PLoS One* **9**, e86033 (2014).
56. Kim, S. W. et al. A sensitive non-radioactive northern blot method to detect small RNAs. *Nucleic acids research* **38**, e98 (2010).
57. Mang, H. G. et al. Abscisic Acid Deficiency Antagonizes High-Temperature Inhibition of Disease Resistance through Enhancing Nuclear Accumulation of Resistance Proteins SNC1 and RPS4 in Arabidopsis. *Plant cell* **24**, 1271–1284 (2012).
58. Kang, H. G. & Klessig, D. F. Salicylic acid-inducible Arabidopsis CK2-like activity phosphorylates TGA2. *Plant Mol. Biol.* **57**, 541–557 (2005).
59. Schneider, C. A., Rasband, W. S. & Eliceiri, K. W. NIH Image to ImageJ: 25 years of image analysis. *Nat. methods* **9**, 671–675 (2012).
60. Louis, J. et al. Discrimination of Arabidopsis PAD4 activities in defense against green peach aphid and pathogens. *Plant Physiol.* **158**, 1860–1872 (2012).
61. Hassan, T. et al. Isolation and identification of cell-specific microRNAs targeting a messenger RNA using a biotinylated anti-sense oligonucleotide capture affinity technique. *Nucleic Acids Res* **41**, e71 (2013).

62. Smith, J. M. & Heese, A. Rapid bioassay to measure early reactive oxygen species production in Arabidopsis leave tissue in response to living Pseudomonas syringae. *Plant Methods* **10**, 6 (2014).
63. Martin, M. Cutadapt removes adapter sequences from high-throughput sequencing reads. *EMBnet.J.* **17** https://doi.org/10.14806/ej.17.1.200 (2011).
64. Cheng, C. Y. et al. Araport11: a complete reannotation of the Arabidopsis thaliana reference genome. *Plant J.* **89**, 789–804 (2017).
65. Kim, D., Paggi, J. M., Park, C., Bennett, C. & Salzberg, S. L. Graph-based genome alignment and genotyping with HISAT2 and HISAT-genotype. *Nat. Biotechnol.* **37**, 907–915 (2019).
66. Li, H. et al. The Sequence Alignment/Map format and SAMtools. *Bioinformatics* **25**, 2078–2079 (2009).
67. Anders, S., Pyl, P. T. & Huber, W. HTSeq–a Python framework to work with high-throughput sequencing data. *Bioinformatics* **31**, 166–169 (2015).
68. Love, M. I., Huber, W. & Anders, S. Moderated estimation of fold change and dispersion for RNA-seq data with DESeq2. *Genome Biol.* **15**, 550 (2014).
69. Chan, P. P. & Lowe, T. M. GtRNAdb 2.0: an expanded database of transfer RNA genes identified in complete and draft genomes. *Nucleic Acids Res*. **44**, D184–D189 (2016).
70. Langmead, B. & Salzberg, S. L. Fast gapped-read alignment with Bowtie 2. *Nat. Methods* **9**, 357–359 (2012).
71. Feng, J., Liu, T., Qin, B., Zhang, Y. & Liu, X. S. Identifying ChIP-seq enrichment using MACS. *Nat. Protoc.* **7**, 1728–1740 (2012).
72. Ellinghaus, D., Kurtz, S. & Willhoeft, U. LTRharvest, an efficient and flexible software for de novo detection of LTR retrotransposons. *BMC Bioinforma.* **9**, 18 (2008).
73. Hsu, C. C. et al. Identification of high-copy number long terminal repeat retrotransposons and their expansion in Phalaenopsis orchids. *BMC Genomics* **21**, 807 (2020).
74. Ou, S. & Jiang, N. LTR_retriever: A Highly Accurate and Sensitive Program for Identification of Long Terminal Repeat Retrotransposons. *Plant Physiol.* **176**, 1410–1422 (2018).
75. Pearson, W. R. & Lipman, D. J. Improved tools for biological sequence comparison. *Proc. Natl. Acad. Sci. USA* **85**, 2444–2448 (1988).
76. Denman, R. B. Using RNAFOLD to predict the activity of small catalytic RNAs. *Biotechniques* **15**, 1090–1095 (1993).
77. Sanchez-Pla, A., Salicrú, M. & Ocana, J. Statistical methods for the analysis of high-throughput data based on functional profiles derived from the gene ontology. *J. Stat. Plan Inference* **137**, 3975–3989 (2007).

Acknowledgements

We thank Daniel.F. Klessig, Georg Jander, D'Maris Dempsey, Chang-Sik Oh, and Angela H. Kang for critical reading on the manuscript, Hailing Jin for *ago2/3/7*, James C. Carrington for *HA-AGO1* and *HA-AGO2* lines, and Dittmar Hahn, Bhavya Doddavarapu and Udayangani Jayasekara for technical assistance. This work was supported by the National Science Foundation (IOS-1553613, H.K.; DBI-1546890, Q.Y.; IOS-1845588, J.L.; MCB 2139857 to X.Z.) and the National Health Institute (R01GM112722, J.K.), the US Department of Agriculture National Institute of Food and Agriculture (Hatch Project TEX0-2-9374, Q.Y.).

Author contributions

S.I.K., Y.B., H.L., D.S.P., P.S.B., J.M., H.C., P.K.Z., P.K., X.Y., and H.G.K. performed the research; H.G.K., S.I.K., Y.B., D.S.P., P.S.B., H.L., J.M., J.K., J.L., X.Z., and Q.Y. analyzed the data; H.G.K. conceived and designed research, and wrote the manuscript, with input from S.I.K., Y.B., H.L., D.S.P., J.M., X.Z., J.L., and Q.Y.

Competing interests

H.G.K. and S.I.K. are named inventors on a patent application related to the subject matter of this publication. The patent, US 2023/0112054, has been published and is currently under review.

Additional information

Supplementary information The online version contains supplementary material available at https://doi.org/10.1038/s42003-025-07737-1.

Correspondence and requests for materials should be addressed to Hong-Gu Kang.

Peer review information This manuscript has been previously reviewed at another Nature Portfolio journal. *Communications Biology* thanks the anonymous reviewers for their contribution to the peer review of this work. Primary Handling Editor: David Favero. A peer review file is available. This document only contains reviewer comments and rebuttal letters for versions considered at *Communications Biology*.